Journal of Materials Chemistry C

ROYAL SOCIETY OF CHEMISTRY

PAPER

View Article Online
View Journal | View Issue

Cite this: J. Mater. Chem. C, 2023, 11, 13095

Tuning the emission and exciton utilization mechanisms of pyrazine-based multi-carbazole emitters and their use in organic light-emitting diodes†‡

Dongyang Chen,[ac] Le Zhang,[ab] Tomas Matulaitis,[a] David B. Cordes,[a] Alexandra M. Z. Slawin,[a] Xiao-Hong Zhang,[c] Ifor D. W. Samuel*[b] and Eli Zysman-Colman*[a]

Thermally activated delayed fluorescence (TADF) and hot excitons are two distinct exciton harvesting mechanisms that can lead to 100% internal quantum efficiency in organic light-emitting diodes (OLEDs). Herein, we show that with judicious molecular engineering, the resulting structurally similar compounds emit *via* distinct photophysical mechanisms, which has a direct consequence on the OLED efficiency. When the pyrazine core is substituted with four carbazoles, the molecule **4CzPyz** shows TADF in doped PPT film, with Φ_{PL} of 75%, ΔE_{ST} of 0.23 eV and τ_d of 150 μs. The device based on **4CzPyz** emits in the sky-blue (λ_{EL} = 486 nm) with an EQE_{max} of 24.1%. When one carbazole is replaced by an *ortho*-biphenyl, the ΔE_{ST} of **3CzBPz** increases to 0.29 eV, the Φ_{PL} decreases to 56%, and the TADF character is largely suppressed in the PPT film. However, a RISC process between higher-lying triplet excited states and the S_1 state is hypothesized to be operational, supported by a combined photophysical and DFT study, to rationalize how the device with **3CzBPz** shows an EQE_{max} of 9.6% (λ_{EL} = 464 nm), reflecting that greater than 86% of the excitons are converted into light in the OLED. When two *ortho*-biphenyl groups are connected to the pyrazine core, the ΔE_{ST} of **2CzBPz** is further increased to 0.34 eV while the Φ_{PL} is reduced to 45% in the PPT film. The DFT and photophysical studies indicate that **2CzBPz** should act as a traditional blue fluorescence emitter. The OLED devices with **2CzBPz** bear this out and exhibit an EQE_{max} 3.2% at a λ_{EL} of 446 nm. These results show how subtle structural changes modulate the efficiency of the triplet exciton harvesting mechanisms and provide new design directions for highly efficient blue emitters for OLEDs.

Received 14th July 2023,
Accepted 4th September 2023

DOI: 10.1039/d3tc02463f

rsc.li/materials-c

Introduction

Reverse intersystem crossing (RISC), is a photophysical process that converts triplet excitons to singlet excitons.[1–3] RISC is central to the thermally activated delayed fluorescence (TADF) mechanism where the process is endothermic and converts non-emissive triplet excitons to emissive singlet excitons.[4–6] Organic light-emitting diodes (OLEDs) with compounds that emit TADF can achieve 100% internal quantum efficiency (IQE).[7,8] For TADF to be operational, the energy gap between the lowest-lying singlet (S_1) and triplet (T_1) excited states, ΔE_{ST}, must be sufficiently small, normally taken to be less than 200 meV.[9,10] The most common design rule for TADF emitters includes poorly electronically coupled electron donor (D) and acceptor (A) moieties in order to confine the highest occupied molecular orbital (HOMO) and lowest unoccupied molecular orbital (LUMO) on the donor and acceptor units, respectively. The resulting small exchange integral induces a small ΔE_{ST}. Using this molecular design requires very electronically weak donor and acceptor groups in order to achieve high-energy emissive S_1 states for blue TADF emitters. Frequently, the limited choice of these groups leads to compounds that show too delocalized frontier molecular orbitals (FMO), leading to

[a] Organic Semiconductor Centre, EaStCHEM School of Chemistry, University of St Andrews, St Andrews, Fife, KY16 9ST, UK.
E-mail: eli.zysman-colman@st-andrews.ac.uk
[b] Organic Semiconductor Centre, SUPA, School of Physics and Astronomy, University of St Andrews, North Haugh, St Andrews, Fife KY16 9SS, UK.
E-mail: idws@st-andrews.ac.uk
[c] Institute of Functional Nano & Soft Materials (FUNSOM), Joint International Research Laboratory of Carbon-Based Functional Materials and Devices, Soochow University, Suzhou, 215123, Jiangsu, P. R. China

† The research data supporting this publication can be accessed at https://doi.org/10.17630/b06557de-c785-4860-bb9e-2d299b2a3eec

‡ Electronic supplementary information (ESI) available. CCDC 2280783–2280785. For ESI and crystallographic data in CIF or other electronic format see DOI: https://doi.org/10.1039/d3tc02463f

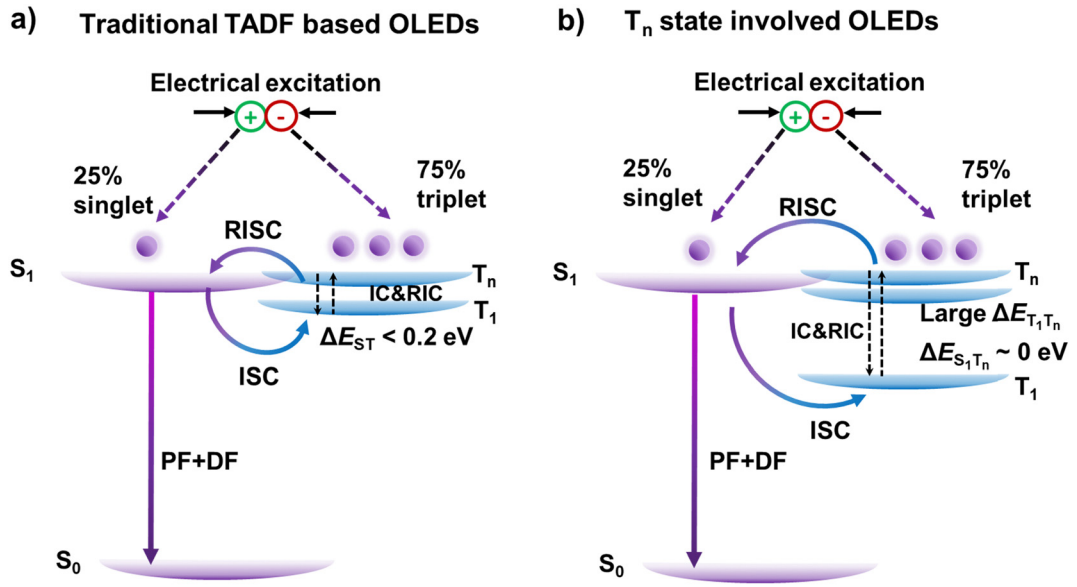

Fig. 1 Illustration of (a) TADF and (b) T_n state involved mechanisms in OLEDs, ISC and RISC are intersystem crossing and reverse intersystem crossing, respectively. PF, DF, IC, and RIC are prompt fluorescence, delayed fluorescence, internal conversion and reverse internal conversion, respectively.

larger ΔE_{ST} and inefficient RISC.[11–13] Meanwhile, the presence of higher-energy triplet states has been suggested to assist in the harvesting of triplet exciton in the device.[14,15] One possible mechanism requires that the higher-energy triplet states T_n ($n > 1$) lie essentially degenerate with S_1 yet be much higher in energy than T_1, which renders RISC competitive with IC.[16–18] The nature of the excited states involved in this mechanism usually show mixed locally-excited (LE) and charge transfer (CT) character [so called hybridized local and charge-transfer (HLCT)] that consequently leads to enhanced spin–orbit coupling between S_1 and these higher-lying triplet states.[14,15] The nature of the HLCT state provides a balance between fast radiative transition rates manifested in high Φ_{PL} and sufficiently small energy gaps between S_1 and T_n ($\Delta E_{S_1T_n}$), facilitating RISC.[16,17]

Compounds emitting *via* either a traditional TADF mechanism, involving RISC between T_1 and S_1 mediated by a small ΔE_{ST}, or emitting *via* a mechanism involving RISC from a T_n state to S_1 ($n > 1$) have been widely explored as emitters for OLEDs (Fig. 1). For TADF emitters based on a twisted D–A structure, the S_1 and T_1 states are usually of CT character, and according to El Sayed's rules, direct RISC from T_1 to S_1 of states with the same orbital symmetry is not allowed, which is reflected in the very low spin–orbit coupling (SOC) between these two states.[19–21] Previous research results have shown that intermediate triplet states between S_1 and T_1 can assist the RISC process, and as the orbital type of T_n usually differs from that of the S_1 state, strong SOC exists.[21–23] Thus, the RISC process is facilitated by spin-vibronic coupling between T_1 and T_n and enhanced SOC between T_n and S_1 when the excited states involved in RISC are energetically closely aligned.[22] Our previous work on the pyrazine-based TADF emitter **DTCz-Pz** also showed that the presence of an intermediate T_2 state of HLCT character that is of different orbital type to S_1 (CT character) can provide an indirect route for RISC to occur despite the relatively large ΔE_{ST} of 0.27 eV in 2,8-bis(diphenylphosphoryl)-dibenzo[b,d]thiophene (PPT).[12] Makhseed *et al.* recently reported a TADF emitter **4CzPyz** where four carbazoles were connected to a pyrazine core, and the multiple carbazoles can present slightly different electronic coupling with the central acceptor, thus providing a dense population of excited states.[24] **4CzPyz** exhibited narrowed ΔE_{ST} of 0.23 eV and shorter delayed lifetime (τ_d) of 144 μs in 10 wt% bis[2-(diphenylphosphino)phenyl]ether oxide (DPEPO) film compared to corresponding values of 0.27 eV and 5.5 ms for **DTCz-Pz** in 7% PPT film.[12,24] However, the electroluminescence behavior of **4CzPyz** was not explored and the increased molecular conjugation caused significantly red-shifted emission as **4CzPyz** showed sky-blue emission with λ_{PL} of 502 nm, while for **DTCz-Pz** which only contains two *tert*-butylcarbazoles were connected to pyrazine, the emission is deep blue with λ_{PL} of 460 nm.[12,24]

ortho-Substituted biphenyl (BP) has been used to improve the RISC process by introducing a LE state in the two-step RISC mechanism without substantially increasing the conjugation in the molecule.[25] The compound **4mCzBN-BP** emits from a CT state [$E(S_1)$ = 2.80 eV] and has a T_1 state of HLCT character [$E(T_1)$ = 2.69 eV] in toluene, both of which are energetically close to the triplet LE state of BP (2.95 eV). As a result, **4mCzBN-BP** exhibited faster k_{RISC} of 2.28×10^6 s^{-1} in toluene, compared to 1.26×10^6 s^{-1} for the reference emitter **4mCzBN**.[25] Inspired by this work, here we modified the reference emitter **4CzPyz** by replacing one or two of the carbazole donors with *ortho*-substituted biphenyl groups and obtained two blue/deep blue emitters, **3CzBPz** and **2CzBPz**. The three compounds exhibit distinct photophysics and exciton harvesting mechanisms in OLEDs. The S_1 energies of **3CzBPz** and **2CzBPz** are destabilized

to 2.94 eV and 3.00 eV, respectively, compared to 2.88 eV for **4CzPyz** in 10 wt% PPT films, while the ΔE_{ST} values progressively increase from 0.23 eV (**4CzPyz**) to 0.29 eV (**3CzBPz**) and 0.34 eV (**2CzBPz**), respectively. The smaller ΔE_{ST} for **4CzPyz** makes it possible to utilize triplet excitons in OLEDs *via* TADF; indeed, the device exhibited a maximum external quantum efficiency (EQE_{max}) of 24.1% and sky-blue emission with λ_{EL} of 486 nm. The close-to-resonant T_3/S_1 states in **3CzBPz** allow the RISC process occurring *via* the higher-energy T_n channels. The OLED with this compound as the emitter shows pure blue emission with λ_{EL} of 464 nm and an EQE_{max} 9.6%. However, the too large ΔE_{ST} for **2CzBPz** precludes either of these two exciton-harvesting mechanisms from being operational and the OLED based on **2CzBPz** exhibits an EQE_{max} of only 3.2% but the device is deep blue with λ_{EL} of 446 nm.

Results and discussion

Synthesis

The synthesis of the three emitters is outlined in Scheme 1. The key intermediate, tetrachloropyrazine, (**4ClPz**) was synthesized in 40% yield from dioxopiperazine upon reaction with phosphorus pentachloride.[25] **4ClPz** was reacted with excess carbazole under S_NAr conditions to obtain **4CzPyz** in a yield of 60%, which is significantly improved compared to the 2.5% previously reported using a Suzuki–Miyaura cross-coupling strategy.[24] For the synthesis of **3CzBPz**, **4ClPz** was converted to the biphenyl-substituted intermediate (**3ClBPz**) *via* a Suzuki–Miyaura reaction, which was then reacted with carbazole to obtain **3CzBPz** in a 70% yield.[26] For the synthesis of **2CzBPz**, **4ClPz** was reacted first with carbazole to obtain the dicarbazole intermediate **2Cz2ClPz**, which was then directly reacted with 2-biphenylboronic acid *via* a Suzuki–Miyaura cross-coupling reaction to obtain **2Cz2BPz** in a yield of 65%.[26] The three emitters were characterized by combination of ^1H and ^{13}C NMR spectroscopy, X-ray diffraction (XRD), high-resolution mass spectrometry, melting point determination, high performance liquid chromatography (HPLC), and elemental analysis. The three emitters have melting points of over 380 °C and high degradation temperatures (T_d for 5 wt% weight loss), measured by thermogravimetric analysis (TGA), of 371, and 420 °C for **2CzBPz** and **4CzPyz** (Fig. S7, ESI‡), respectively. For **3CzBPz** sublimation was, however, observed during the TGA, and the temperature responsible for 5 wt% weight loss is 407 °C.

Single crystals of **4CzPyz** were grown *via* slow evaporation of a mixed solution of chloroform/methanol, while single crystals of **3CzBPz** and **2CzBPz** were obtained following gradient-temperature vacuum sublimation. The structures are illustrated in Fig. 2. The three compounds show similar degrees of twist of the carbazole rings away from the plane of the central pyrazine, **4CzPyz** and **3CzBPz** being the most similar. In **4CzPyz** the carbazole groups are twisted slightly differently depending on which side of the pyrazine ring they are on. In the first independent molecule, one side shows dihedral angles between the pyrazine and the mean plane of the carbazole of 34.67° and 43.18°, the other of 49.68° and 54.20°. The second independent molecule shows a less extreme difference, one side showing angles of 42.91° and 43.45°, the other of 55.09° and 56.73°. For **3CzBPz**, the carbazole at the *ortho* position to the biphenyl is twisted with a dihedral angle of 47.39°, while the dihedral angles for the carbazoles at the *meta* and *para* positions are larger at 56.01° and 52.71°, respectively. The dihedral angle between the carbazoles and the pyrazine in **2CzBPz** are at the higher end of the range seen, at 55.06°, rather different to those of a previously reported green-emissive pyrazine-containing TADF emitter **pDTCz-DPzS** [38.20(8)°].[7] As was the case for the previously reported structure of the DMF

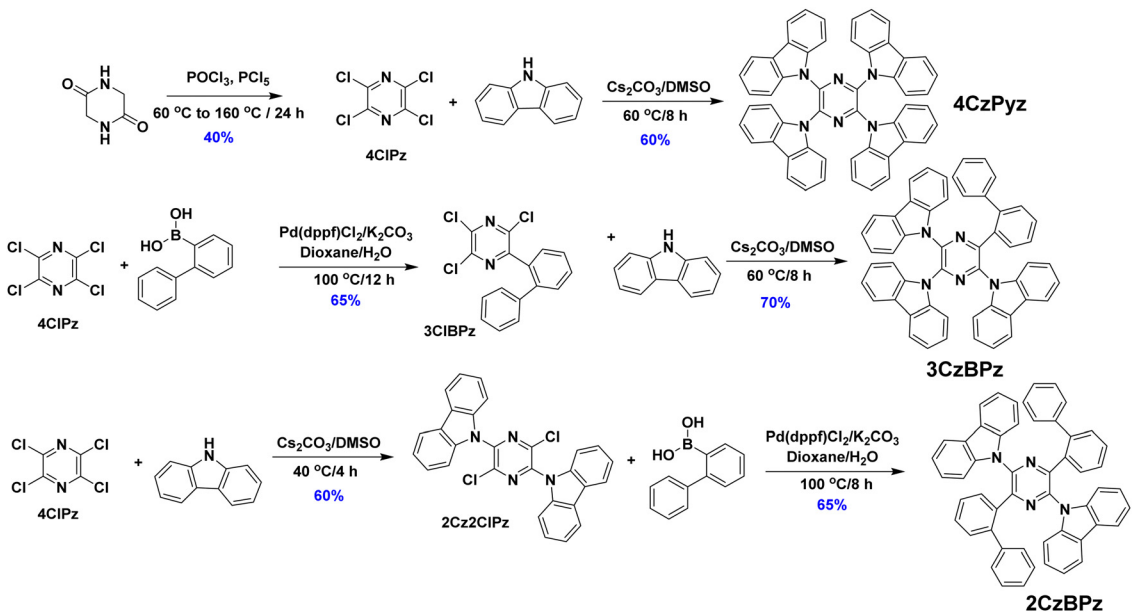

Scheme 1 Synthesis route of **4CzPyz**, **3CzBPz**, and **2CzBPz**.

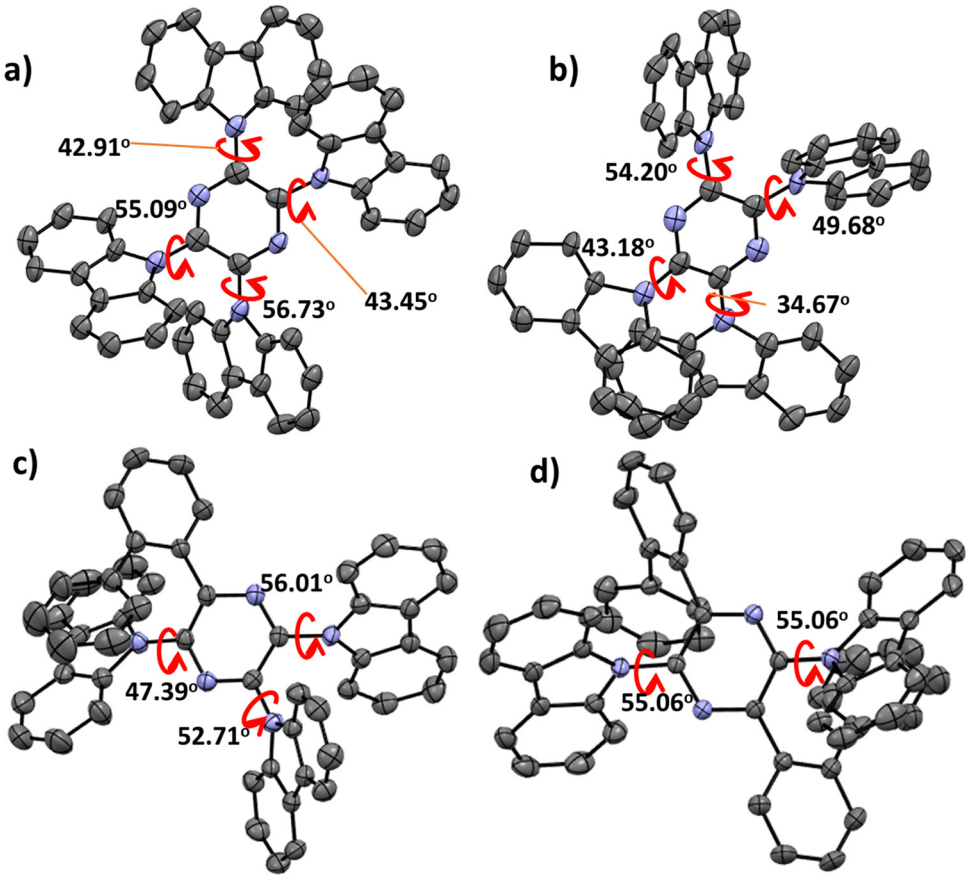

Fig. 2 Thermal ellipsoid plots of the crystal structures of (a) and (b) the two independent molecules of **4CzPyz**, (c) **3CzBPz**, and (d) **2CzBPz**. Ellipsoids are drawn at the 50% probability level, and minor components of disorder and hydrogens are omitted for clarity.

solvate of **4CzPyz**,[27] the crystal structure of **4CzPyz** shows several intermolecular C–H···π interactions with H···centroid distances between 2.53 and 2.67 Å and corresponding C···centroid distances between 3.425(9) and 3.593(10) Å (Fig. S8, ESI‡). The structure of **3CzBPz** also showed some C–H···π interactions, with H···centroid distances of 2.69 Å and corresponding C···centroid distances of 3.6002(18) Å. This close packing mode is not observed in **2CzBPz**.

Theoretical calculations

Optimization of the ground state geometries of the three emitters was carried out by DFT calculation at the PBE0/6-31G(d,p) level of theory, starting from the X-ray crystal structures.[28,29] The Tamm–Dancoff approximation (TDA) to TD-DFT was applied to investigate the character of both the excited singlet and triplet states as well as to estimate ΔE_{ST}.[28] The spin–orbital coupling matrix element (SOCME) values between excited states were obtained using PySOC based on the optimized triplet state geometries.[30] The HOMO of **4CzPyz** is distributed across the whole molecule while the LUMO is mainly localized on the pyrazine, whereas for **3CzBPz** and **2CzBPz**, the HOMOs are located on the carbazole moieties and the pyrazine, while LUMOs are delocalized on pyrazine and the biphenyl substituent. The HOMOs for the three emitters are predicted to be around −5.50 eV, while the LUMOs for **3CzBPz** and **2CzBPz** are destabilized to −1.62 eV and −1.60 eV, respectively, compared to −1.72 eV for **4CzPyz**, which hints that the delocalization of the pyrazine weakens the electron-withdrawing character of the acceptor. The TDA-DFT calculations predict the three emitters to have similar, moderately large ΔE_{ST} values of around 0.40 eV. For **4CzPyz**, the S_1 and T_1 are 3.09 eV and 2.56 eV, respectively, and the intermediate T_2 (2.99 eV) is energetically close to S_1 (Fig. 3). Moreover, the nature of T_2 is of HLCT character and different from the CT dominant character of S_1 and T_1, which leads to a much higher SOCME value ($H_{SOC}^{S_1T_2} = 0.47\ cm^{-2}$) between T_2 and S_1 than $2 \times 10^{-4}\ cm^{-2}$ for direct SOC between T_1 and S_1 (Fig. S1, ESI‡). The S_1 and T_1 of **3CzBPz** are destabilized, respectively, to 3.17 eV and 2.65 eV, both of which show dominant CT character, while the T_2 is 2.99 eV and T_3 is degenerated to S_1 at 3.19 eV, both possessing HLCT character. T_3 and S_1 exhibits the highest SOC with $H_{SOC}^{S_1T_3}$ of 1.21 cm^{-2} compared to 1.18 cm^{-2} and 0.45 cm^{-2} for $H_{SOC}^{S_1T_2}$ and $H_{SOC}^{S_1T_1}$, respectively (Fig. S2, ESI‡). The high SOC and small energy gap (0.02 eV) between S_1 and T_3 indicate that RISC in **3CzBPz** can occur between T_3 and S_1 *via* high-energy triplet state mechanism.[18] The S_1 and T_1 of **2CzBPz** are 3.18 eV and 2.67 eV, respectively, both of which show dominant CT

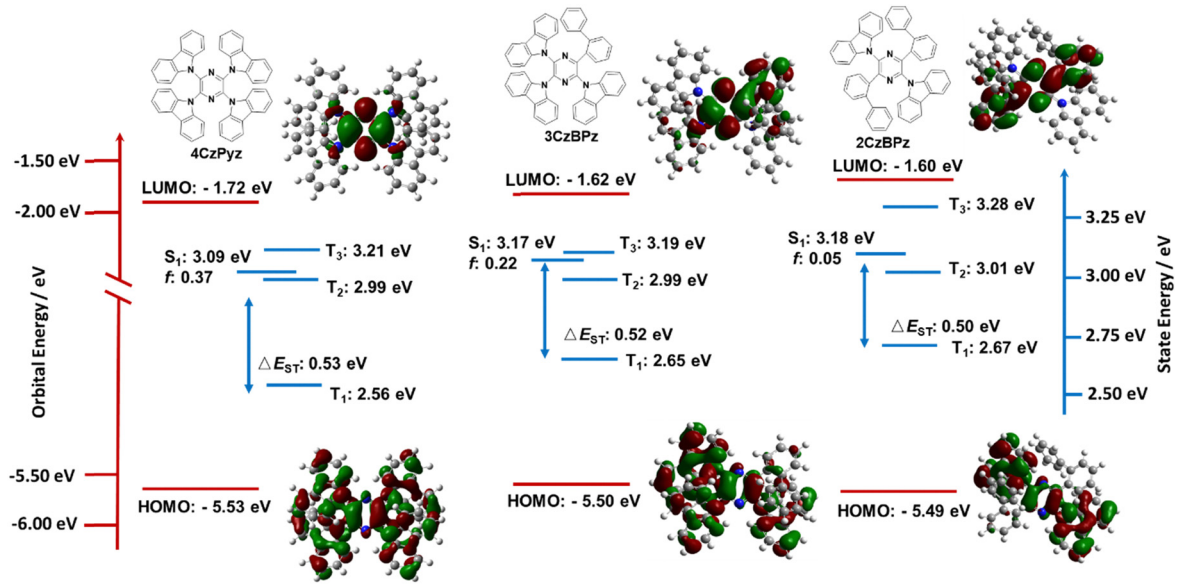

Fig. 3 Theoretical modelling of the energies of the HOMO/LUMO and the S_1 and T_1 states of **4CzPyz**, **3CzBPz**, and **2CzBPz** in the gas phase and the electron density distribution of the frontier molecular orbitals at PBE0/6-31G(d,p) level (isovalue = 0.02).

character. The T_2 and T_3 of **2CzBPz** are 3.01 eV and 3.28 eV, and the energy offset between S_1/T_2 (0.17 eV) or S_1/T_3 (0.10 eV) seems to reduce RISC processes involving these states greatly, with the ΔE_{ST} also too large, this compound is predicted to be fluorescent.

Electrochemistry

Cyclic voltammetry (CV) and differential pulse voltammetry (DPV) measurements of **4CzPyz**, **3CzBPz**, and **2CzBPz** were carried out in DCM with tetrabutylammonium hexafluorophosphate (n-Bu_4NPF_6) as the supporting electrolyte to estimate the HOMO and LUMO energies (Fig. 4). The CV traces of **4CzPyz**, **3CzBPz**, and **2CzBPz** show irreversible oxidation waves with E_{pa}s of 1.16 V, 1.08 V and 1.07 V, respectively, which align with the corresponding oxidation potentials obtained from the DPV of E_{ox} = 1.12 V, 1.07 V, and 1.08 V, respectively. **4CzPyz** possesses a pseudo-reversible reduction wave with E_{pc} of −1.80 V which aligns with the reduction potential E_{red} = −1.76 V obtained from the DPV, while no reduction waves are observed for **3CzBPz** and **2CzBPz** within the DCM solvent window. The corresponding HOMO levels of **4CzPyz**, **3CzBPz** and **2CzBPz** inferred from the E_{ox} values in the DPVs are −5.46 eV, −5.41 eV and −5.42 eV, respectively, which are slightly stabilized than those predicted from the DFT calculations yet match the calculated trend. The HOMO value of **4CzPyz** (−5.46 eV) is slightly destabilized compared to the reported value of −5.59 eV in DCM.[24] The LUMO level of **4CzPyz** is −2.58 eV, which is moderately destabilized compared to the reported value of −2.83 eV in DCM,[24] while the LUMO levels for **3CzBPz** and **2CzBPz** are calculated to be −2.47 eV and −2.45 eV, respectively, where these are inferred from the HOMO energies and the optical gaps (E_g), which themselves were determined from the intersection of the normalized absorption and

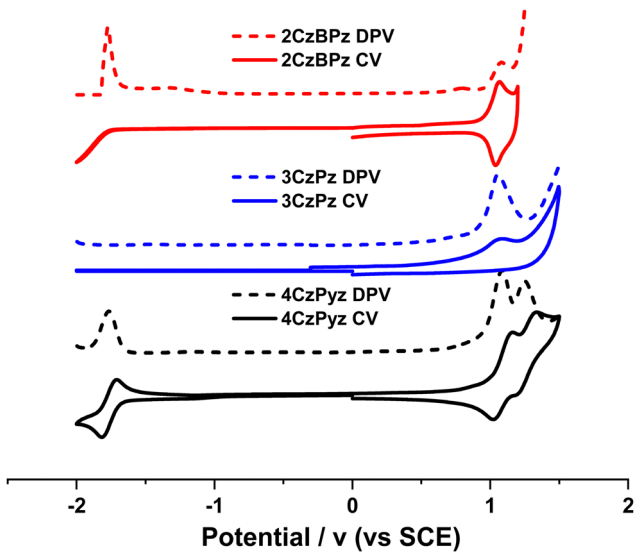

Fig. 4 CV (solid lines) and DPV (dashed lines) for **4CzPyz**, **3CzBPz**, and **2CzBPz** in degassed DCM solution containing [nBu$_4$N]PF$_6$ as the supporting electrolyte and using Fc/Fc$^+$ as an external standard (Fc/Fc$^+$ = 0.46 eV *versus* SCE,[31] scan rate = 100 mV s^{-1}).

fluorescence spectra in toluene (2.94 eV and 2.97 eV, Fig. S5d, ESI‡). The LUMOs values of **4CzPyz**, **3CzBPz** and **2CzBPz** are moderately more stabilized than the values obtained from DFT calculations, yet follow the calculated trend.

Photophysics

The UV-vis absorption spectra of **4CzPyz**, **3CzBPz**, and **2CzBPz** in toluene are shown in Fig. 5. The profiles match closely to the TDA-DFT calculated absorption spectra (Fig. S4, ESI‡). The TDA-DFT calculations predict that the S_1 of the three emitters

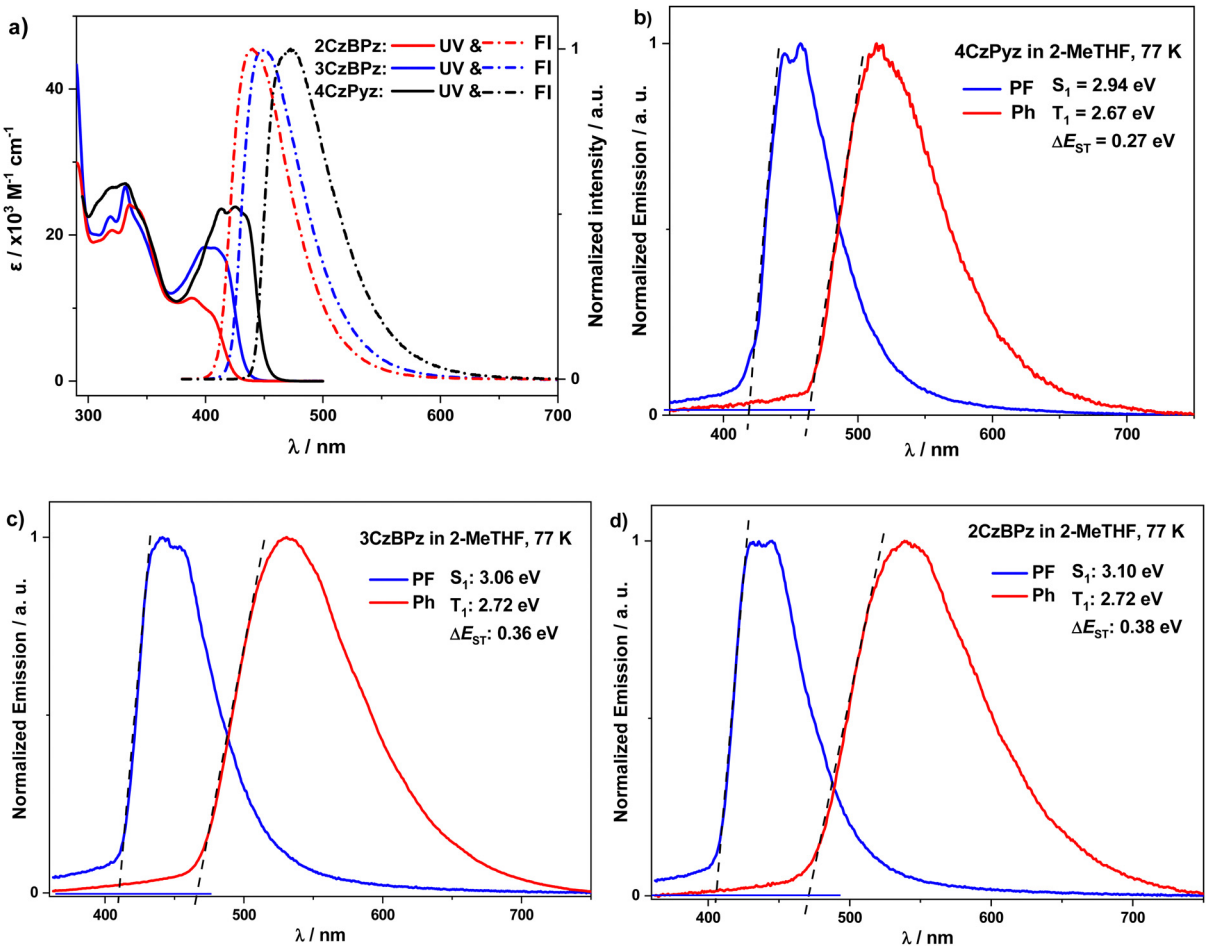

Fig. 5 (a) Absorption (solid) and emission (dashed) spectra of **4CzPyz**, **3CzBPz**, and **2CzBPz** in toluene solution (λ_{exc} = 380 nm), prompt fluorescence (Fl) (1–100 ns) and phosphorescence (Ph) (1–10 ms) spectra of (a) **4CzPyz**, (b) **3CzBPz** and (c) **2CzBPz** at 77 K in 2-MeTHF (λ_{exc} = 343 nm).

should exhibit charge-transfer dominated hybrid transitions from HOMO to LUMO (Fig. S1–S3, ESI‡). **4CzPyz**, **3CzBPz**, and **2CzBPz** all exhibit structured absorption around 450–380 nm. **4CzPyz** showed the strongest hybrid CT absorption with molar absorptivity (ε) values of 2.4×10^4 M^{-1} cm^{-1} (425 nm) and 2.3×10^4 M^{-1} cm^{-1} (413 nm), while for **3CzBPz** the absorption band is less intense and blue-shifted to 1.8×10^4 M^{-1} cm^{-1} (408 nm) and 1.7×10^4 M^{-1} cm^{-1} (398 nm). The absorption of **2CzBPz** is further attenuated and blue-shifted, with ε of 0.9×10^4 M^{-1} cm^{-1} (401 nm) and 1.1×10^4 M^{-1} cm^{-1} (388 nm). The tendency of the ε values match the TDA-DFT results where the oscillator strengths (f) reduce from 0.37 for **4CzPyz** to 0.22 and 0.05 for **3CzBPz** and **2CzBPz**, respectively. The three compounds exhibit structureless emission in toluene with λ_{PL} of 473 nm, 450 nm, and 440 nm for **4CzPyz**, **3CzBPz**, and **2CzBPz**, respectively. The blue-shifted emission of **3CzBPz**, and **2CzBPz** are ascribed to the weaker character of the acceptors. The three emitters exhibit a moderately high Φ_{PL} in degassed toluene, of 71%, 65%, and 64% for **4CzPyz**, **3CzBPz**, and **2CzBPz**, respectively, which are slightly reduced to 66%, 63%, and 61% after exposure to oxygen. The S_1 and T_1 values were extracted from the onsets of the fluorescence and phosphorescence spectra, respectively, in 2-methyltetrahydrofuran (2-MeTHF) glass at 77 K (Fig. 5(b)–(d)). At 77 K, the three emitters exhibit broad and featureless fluorescence as well as phosphorescence spectra, which suggest that both of these states possess mainly CT character. The S_1/T_1 states for **4CzPyz**, **3CzBPz**, and **2CzBPz** are measured to be 2.94/2.67 eV, 3.06/2.72 eV, and 3.10/2.72 eV, respectively, which match the tendency of TDA-DFT calculation, and the corresponding ΔE_{ST} values are 0.27 eV, 0.36 eV, and 0.38 eV, respectively.

The time-resolved PL decays of these materials were measured in 10^{-5} M degassed toluene solution (Fig. 6(a)). **4CzPyz**, **3CzBPz**, and **2CzBPz** exhibit prompt lifetime (τ_p) of 6.4 ns, 4.3 ns, and 6.8 ns, respectively; however, no delayed component was detected. The PL decay and oxygen insensitivity behavior of **4CzPyz**, **3CzBPz** and **2CzBPz** in toluene indicate that in toluene these compounds behave as fluorophores only. As the TDA-DFT calculations indicated that a HLCT triplet exciton harvesting mechanism may be possible in **4CzPyz** and **3CzBPz**, we examined the effect of solvent polarity on the nature of the excited state (Fig. S5, ESI‡) by undertaking a Lippert–Mataga study for each of the three emitters. All materials showed emission that was insensitive to polarity changes in low-polarity solvents,

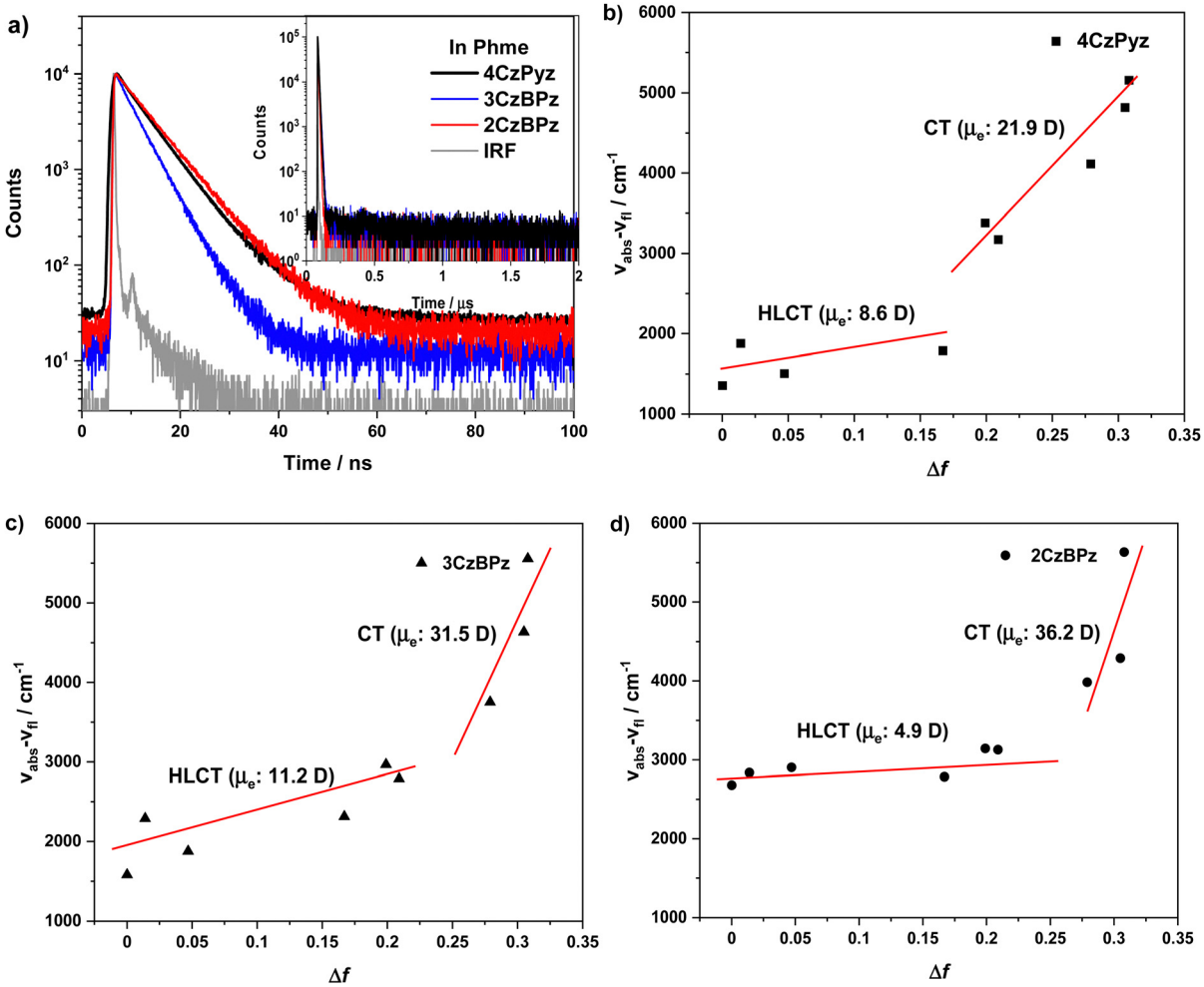

Fig. 6 (a) transient PL decay curves of three emitters in toluene (λ_{exc} = 379 nm), and solvatochromic Lippert–Mataga plots for (b) **4CzPyz**, c() **3CzBPz**, and **2CzBPz**.

such as cyclohexane, and showed broadened emission in high-polarity solvents such as acetonitrile and methanol. The behaviour is a hallmark of compounds with low-lying HLCT excited states. The Stokes shift *versus* the orientation polarizability (Δf) plots as well as the electric dipole moment (μ_e) of three emitters are presented in Fig. 6(b)–(d). Notably, the Lippert–Mataga plots of three emitters each show two regions where there is a linear relationship between solvent polarity and Stokes shift, indicative of compounds possessing excited states of mixed LE/CT character. The Lippert–Mataga plots reveal that the three emitters show increased CT character in high polarity solvents while in low polarity solvents the S_1 states possess more significant LE character. The smaller degree of red-shifting of the emission spectra and smaller μ_e in **2CzBPz** suggest that there is greater LE character to the S_1 state in this compound than in **3CzBPz** and **4CzPyz**.

With a view to using these compounds as emitters in OLEDs, we then investigated the photophysics of the three emitters in solid-state matrices. The photoluminescence spectra of three emitters are insensitive to the medium, with λ_{PL} of 486 nm, 463 nm, and 446 nm for **4CzPyz**, **3CzBPz** and **2CzBPz** (Fig. 7(a)), which are only modestly red-shifted compared to the corresponding λ_{PL} of 473 nm, 450 nm, and 440 nm in toluene, respectively. The highest Φ_{PL} value for **4CzPyz** was achieved in 10 wt% doped PPT film at 75%, which is significantly higher than the 36% previously reported in the 10 wt% doped DPEPO film.[24] The Φ_{PL} values for **3CzBPz** and **2CzBPz** in PPT are 56%, and 38%, respectively, which are slightly lower than corresponding values in DPEPO (Fig. 7(b)). The tendency of the Φ_{PL} of the three emitters match the TDA-DFT calculated trend in oscillator strength.

The three emitters in 10 wt% doped PPT films exhibit unstructured emission, with FWHM of 64 nm, 63 nm and 44 nm for **4CzPyz**, **3CzBPz** and **2CzBPz**, respectively, and the phosphorescence is of dominant CT character with broader (FWHM ~ 120 nm) and featureless emission (Fig. 7). The calculated ΔE_{ST} values of the three emitters determined from the onsets of the prompt fluorescence and phosphorescence spectra, are 0.23 eV (same value as previously reported in DPEPO),[24] 0.29 eV, and 0.34 eV for **4CzPyz**, **3CzBPz** and **2CzBPz** (Fig. 8), respectively.

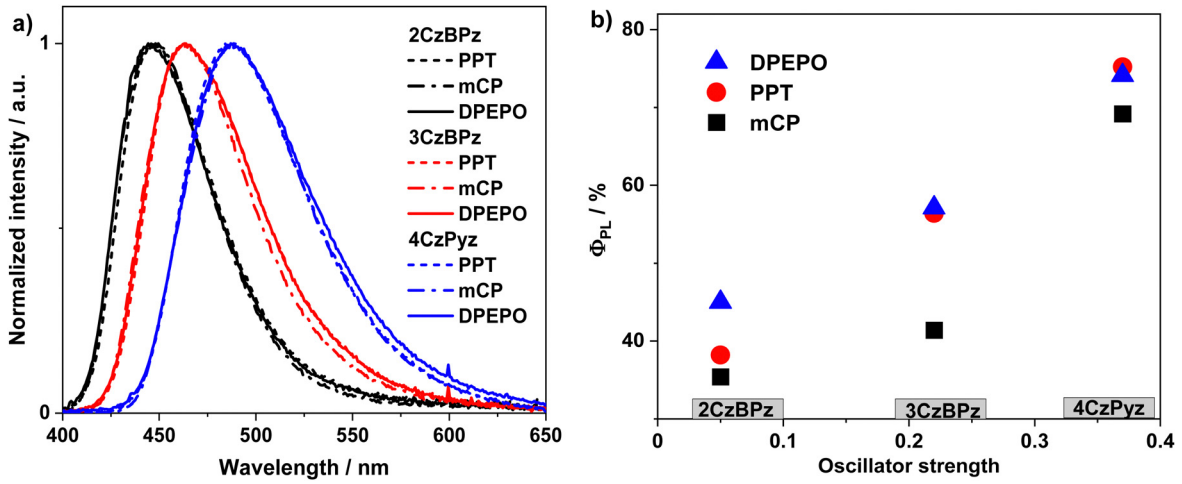

Fig. 7 (a) Emission spectra and (b) Φ_{PL} of **4CzPyz**, **3CzBPz**, and **2CzBPz** in 10 wt% doped hosts (λ_{exc} = 310 nm).

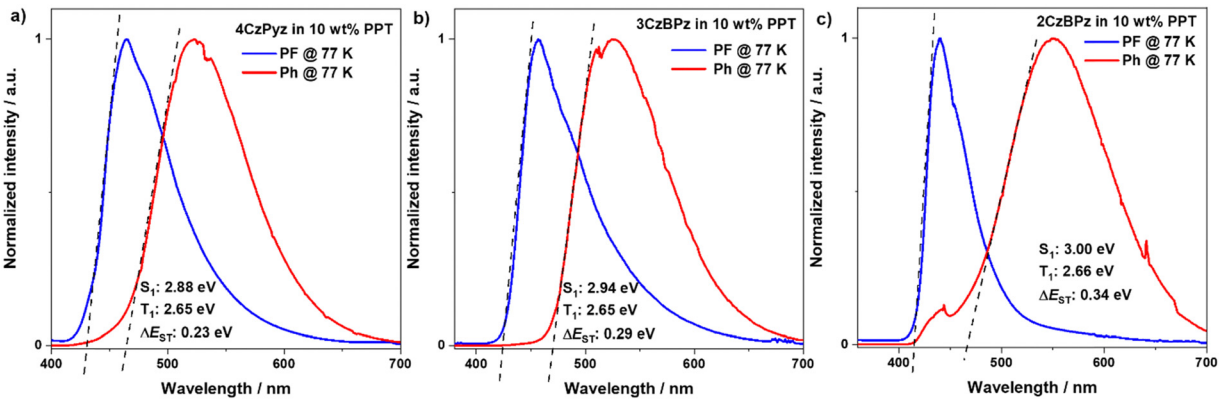

Fig. 8 Prompt fluorescence (PF) at 77 K (delay: 1 ns, gate: 100 ns), and phosphorescence spectra at 77 K (delay: 2 ms, gate: 4 ms) of (a) **4CzPyz**, (b) **3CzBPz** and (c) **2CzBPz** in 10 wt% doped PPT film (λ_{exc} = 343 nm).

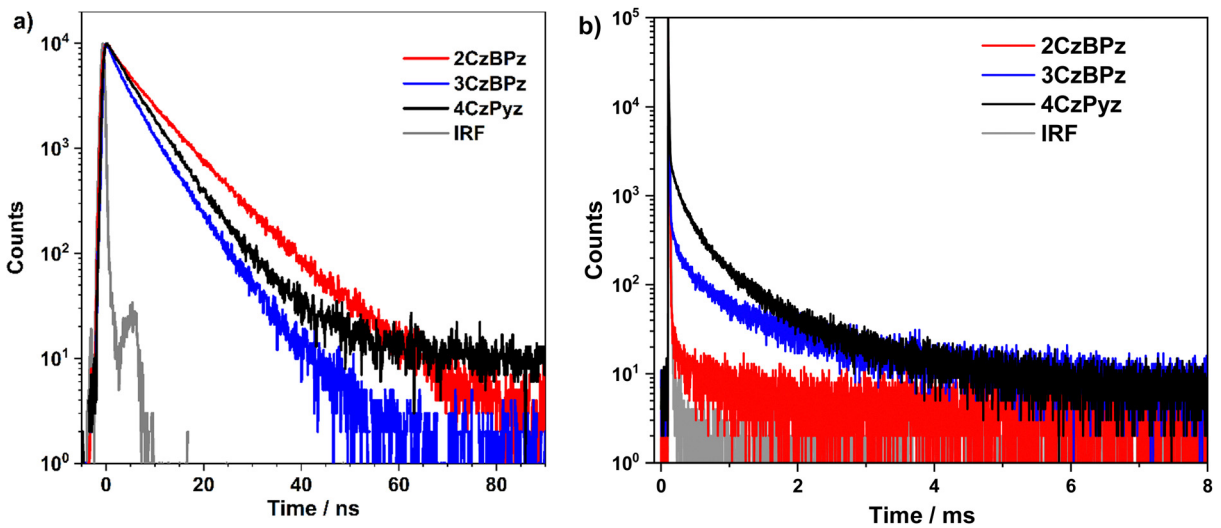

Fig. 9 Transient PL decay curves of **4CzPyz**, **3CzBPz**, and **2CzBPz** in 10 wt% doped PPT films in (a) 100 ns time window and (b) 8 ms time window (λ_{exc} = 378 nm).

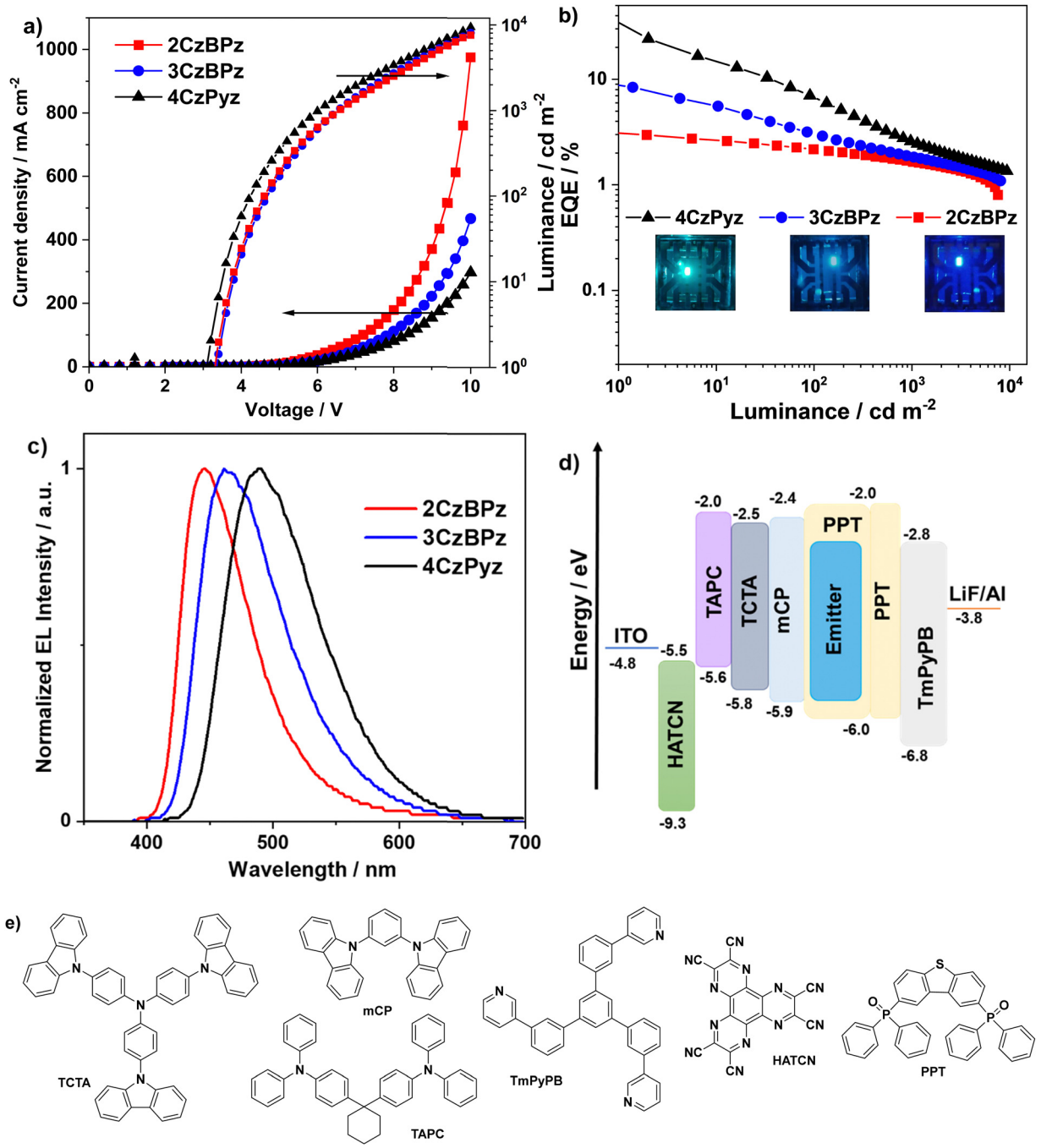

Fig. 10 Optimized devices based on **4CzPyz**, **3CzBPz**, and **2CzBPz**: (a) current density–voltage–luminance characteristics, (b) EQE–luminance characteristics, (c) EL spectra, (d) energy level diagram of the device structure, (e) molecular structures of the materials used in the device.

The room temperature time-resolved PL decays in 10 wt% doped PPT films are shown in Fig. 9. The prompt fluorescence decays of the three emitters show bi-exponential kinetics with τ_{avg} of 5.9, 5.1, and 7.6 ns for **4CzPyz**, **3CzBPz** and **2CzBPz** (Fig. 9(a)), respectively. The doped films of **4CzPyz** and **3CzBPz** show delayed emission, with delayed lifetimes, τ_d (Fig. 9(b)) of 150 μs for **4CzPyz** (the lifetime reported in the literature was 174 μs),[24] and 929 μs for **3CzBPz**. The intensity of the delayed emission increases with increasing temperature (Fig. S6, ESI‡). The smaller ΔE_{ST} and the temperature dependence of the delayed component from **4CzPyz** indicates that the compound in a 10 wt% doped film in PPT shows TADF. The weak TADF of the **3CzBPz** doped film in PPT film can also be triggered with the assistance of higher-energy triplet excited states despite the larger ΔE_{ST} of 0.29 eV. However, there is no indication of TADF in **2CzBPz** due to the too large ΔE_{ST} of 0.34 eV.

Electroluminescence properties

Next, we investigated the electroluminescence properties of these three emitters. Multilayer OLEDs were fabricated using

these materials as dopants within the emissive layer, with the following device structures: ITO/HATCN (5 nm)/TAPC (40 nm)/TCTA (10 nm)/*m*CP (10 nm)/PPT: emitter (10 wt%) (30 nm)/PPT (10 nm)/TmPyPB (40 nm)/LiF (0.8 nm) Al (100 nm). Here, HATCN acts as the hole injection layer, TAPC and TCTA are used as hole transporting layers, and *m*CP is the exciton blocking layer. PPT was selected as the host material due to the good carrier transport ability and the high Φ_{PL} values of the three emitters in 10 wt% doped films, and TmPyPB is the electron-transporting material. The performance of the devices is summarized in Fig. 10. The devices based on the three emitters exhibit turn on voltage (V_{on}) at 3.0 V, and the maximum luminance (Lum_{max}) exceeded 10^4 cd m^{-2}. The OLEDs based on **4CzPyz** exhibit sky blue emission with λ_{EL} of 486 nm, and CIE coordinates of (0.20, 0.36). Thanks to the high Φ_{PL} and TADF character of **4CzPyz** in PPT host (Fig. 7(b) and 9(b)), a maximum EQE (EQE_{max}) of 24.1% is achieved at 3 cd m^{-2}, which is much higher than our previously reported pyrazine-based TADF emitter **DTCz-Pz** (EQE_{max}: 11.6% at 2 cd m^{-2}). The EQE reduced to 7.0% and 2.6% at 100 cd m^{-2} and 1000 cd m^{-2}, respectively. For OLEDs with **3CzBPz**, blue emission is achieved with λ_{EL} of 464 nm and CIE coordinates of (0.16, 0.22). The EQE_{max} for the device with **3CzBPz** reached 9.6% at 1 cd m^{-2} and this reduced to 3.1% and 2.0% at 100 cd m^{-2} and 1000 cd m^{-2}, respectively. The severe efficiency roll-off of the devices with **4CzPyz** and **3CzBPz** are ascribed to the relatively larger ΔE_{ST} values and thus longer triplet exciton lifetimes, a correlation that has also been noted in previously reported pyrazine- or pyrimidine-based blue emitters (Table S3, ESI‡).[12,32–34]

The EQE is a product of four parameters and can be expressed as:

$$EQE = \gamma \Phi_F \eta_{S/T} \eta_{out} \quad (1)$$

where γ represents the charge carrier balance of the device, Φ_{PL} is the photoluminescence quantum efficiency of the emitter, $\eta_{S/T}$ accounts for the ratio of excitons that are able to decay radiatively, and η_{out} is the outcoupling efficiency. Considering the Φ_{PL} of 56% in **3CzBPz** doped PPT film and presuming 20% of typical light outcoupling for OLEDs and 100% for hole–electron combination efficiency, the $\eta_{S/T}$ of the **3CzBPz** based OLEDs reaches 86%, and the slightly sub-linear relationship between luminance and current density of the device with **3CzBPz** (Fig. S7, ESI‡) rules out triplet–triplet annihilation (TTA) as a dominant exciton harvesting process in the OLED.[3,35] The device results are consistent with a higher energy triplet state being involved in the exciton harvesting mechanism. The high EQE_{max} value also makes **3CzBPz** amongst the most efficient HLCT emitters (Table S4, ESI‡). The device based on **2CzBPz** exhibited deep blue emission with λ_{EL} of 446 nm and CIE coordinates of (0.15, 0.12). The EQE_{max} for the OLED with **2CzBPz** is 3.2%. The $\eta_{S/T}$ for **2CzBPz** device is estimated to be 42%, indicating only a small portion of triplet excitons are utilized in OLEDs based **2CzBPz**. The λ_{EL} of the devices with **4CzPyz**, **3CzBPz**, and **2CzBPz** are progressively blue-shfited at 486 nm, 464 nm, and 446 nm, respectively, values that are almost identical to the corresponding λ_{PL} in the PPT film (Fig. 7(a) and 10(c)).

Conclusions

We investigated the excited state dynamics, photophysical properties, and exciton utilization mechanism in OLEDs of three pyrazine-based multi-carbazole containing emitters through a combined, detailed theoretical and experimental study. When four carbazoles are connected to the pyrazine core, the emitter **4CzPyz** exhibits a moderate ΔE_{ST} of 0.23 eV, high Φ_{PL} of 74% and TADF character (τ_p: 5.9 ns, τ_d: 150 μs) in PPT film. The device based on **4CzPyz** shows sky-blue emission (λ_{EL} = 486 nm) with EQE_{max} of 24.1% thanks to the highly efficient exciton utilization by TADF mechanism. When one carbazole is replaced by an *ortho*-biphenyl, the ΔE_{ST} of **3CzBPz** is increased to 0.29 eV, Φ_{PL} decreases to 57%, and the TADF character is lost in PPT film. However, the photophysical properties and DFT calculations support that **3CzBPz** can harvest triplet excitons *via* a higher-energy triplet state channel mechanism. This is reflected also in the OLED performance where the device shows an EQE_{max} of 9.6% at λ_{EL} of 464 nm; indeed, 86% of the excitons are estimated to be converted into light in the OLED based on **3CzBPz**. When two *ortho*-biphenyl groups are connected to the pyrazine core, the ΔE_{ST} of **2CzBPz** is further increased to 0.34 eV and Φ_{PL} is reduced to 45% in PPT film. The calculations and photophysics indicate **2CzBPz** to be a deep blue fluorescence emitter, and the OLEDs based on **2CzBPz** exhibits an EQE_{max} 3.2% with λ_{EL} of 446 nm. These results show the critical role of a suitably aligned LE triplet state in modulating the nature of the exciton harvesting mechanism, leading to dramatically different efficiencies in the OLEDs.

Conflicts of interest

There are no conflicts to declare.

Acknowledgements

The St Andrews team would also like to thank EPSRC (EP/P010482/1 and EP/L017008/1) for financial support. EZ-C is a Royal Society Leverhulme Trust Senior Research Fellow (SRF\R1\201089). D.C thanks the China Postdoctoral Science Foundation (No. 2022TQ0227).

References

1 C. M. Marian, *Annu. Rev. Phys. Chem.*, 2020, **72**, 617–640.
2 T. J. Penfold, E. Gindensperger, C. Daniel and C. M. Marian, *Chem. Rev.*, 2018, **118**, 6975–7025.
3 R. Ieuji, K. Goushi and C. Adachi, *Nat. Commun.*, 2019, **10**, 13044.
4 Y.-Z. Shi, H. Wu, K. Wang, J. Yu, X.-M. Ou and X.-H. Zhang, *Chem. Sci.*, 2022, **13**, 3625–3651.

5 J. Teng, Y. Wang, C. Chen, J. Teng and Y. Wang, *J. Mater. Chem. C*, 2020, **8**, 11340–11353.
6 X. K. Chen, D. Kim and J. L. Brédas, *Acc. Chem. Res.*, 2018, **51**, 2215–2224.
7 P. L. dos Santos, D. Chen, P. Rajamalli, T. Matulaitis, D. B. Cordes, A. M. Z. Slawin, D. Jacquemin, E. Zysman-Colman and I. D. W. Samuel, *ACS Appl. Mater. Interfaces*, 2019, **11**, 45171–45179.
8 D. Sun, E. Duda, X. Fan, R. Saxena, M. Zhang, S. Bagnich, X. Zhang, A. Köhler and E. Zysman-Colman, *Adv. Mater.*, 2022, **34**, 2110344.
9 P. Xiao, J. Huang, Y. Yu, J. Yuan, D. Luo, B. Liu and D. Liang, *Appl. Sci.*, 2018, **8**, 1–27.
10 F. B. Dias, K. N. Bourdakos, V. Jankus, K. C. Moss, K. T. Kamtekar, V. Bhalla, J. Santos, M. R. Bryce and A. P. Monkman, *Adv. Mater.*, 2013, **25**, 3707–3714.
11 Q. Zhang, J. Li, K. Shizu, S. Huang, S. Hirata, C. Adachi, P. C. Adachi, Q. Zhang, J. Li, K. Shizu, S. Hirata and H. Miyazaki, *J. Am. Chem. Soc.*, 2012, **134**, 14706–14709.
12 P. Rajamalli, D. Chen, S. M. Suresh, Y. Tsuchiya, C. Adachi and E. Zysman-Colman, *Eur. J. Org. Chem.*, 2021, 2285–2293.
13 L. S. Cui, H. Nomura, Y. Geng, J. U. K. Kim, H. Nakanotani and C. Adachi, *Angew. Chem., Int. Ed.*, 2017, **56**, 1571–1575.
14 G. Sun, X. H. Wang, J. Li, B. T. Yang, Y. Gao and Y. Geng, *Sci. Rep.*, 2021, **11**, 17686–17688.
15 T. Liu, X. Chen, J. Zhao, W. Wei, Z. Mao, W. Wu, S. Jiao, Y. Liu, Z. Yang and Z. Chi, *Chem. Sci.*, 2021, **12**, 5171–5176.
16 D. Hu, L. Yao, B. Yang and Y. Ma, *Philos. Trans. R. Soc., A*, 2015, **373**, 20140318.
17 Y. Xu, P. Xu, D. Hu and Y. Ma, *Chem. Soc. Rev.*, 2021, **50**, 1030–1069.
18 N. Sharma, M. Y. Wong, D. Hall, E. Spuling, F. Tenopala-Carmona, A. Privitera, G. Copley, D. B. Cordes, A. M. Z. Slawin, C. Murawski, M. C. Gather, D. Beljonne, Y. Olivier, I. D. W. Samuel and E. Zysman-Colman, *J. Mater. Chem. C*, 2020, **8**, 3773–3783.
19 M. A. El-Sayed, *J. Chem. Phys.*, 1963, **38**, 2834–2838.
20 H. Noda, H. Nakanotani and C. Adachi, *Sci. Adv.*, 2018, **4**, eaao6910.
21 M. K. Etherington, J. Gibson, H. F. Higginbotham, T. J. Penfold and A. P. Monkman, *Nat. Commun.*, 2016, **7**, 13680.
22 H. Noda, X. Chen, H. Nakanotani, T. Hosokai, M. Miyajima, N. Notsuka, Y. Kashima, J. Brédas and C. Adachi, *Nat. Mater.*, 2019, **18**, 1084–1090.
23 J. U. Kim, I. S. Park, C. Chan, M. Tanaka, H. Nakanotani and C. Adachi, *Nat. Commun.*, 2020, **11**, 1765.
24 L. Salah, M. K. Etherington, A. Shuaib, A. Danos, A. A. Nazeer, B. Ghazal, A. Prlj, A. T. Turley, A. Mallick, P. R. McGonigal, B. F. E. Curchod, A. P. Monkman and S. Makhseed, *J. Mater. Chem. C*, 2021, **9**, 189–198.
25 S. J. Woo, Y. H. Ha, Y. H. Kim and J. J. Kim, *J. Mater. Chem. C*, 2020, **8**, 12075–12084.
26 T. Ishiyama, M. Murata and N. Miyaura, *J. Org. Chem.*, 1995, **60**, 7508–7510.
27 L. Salah, M. K. Etherington, A. Shuaib, A. Danos, A. A. Nazeer, B. Ghazal, A. Prlj, A. T. Turley, A. Mallick, P. R. McGonigal, B. F. E. Curchod, A. P. Monkman and S. Makhseed, *J. Mater. Chem. C*, 2021, **9**, 189–198.
28 J. A. Pople, J. S. Binkley and R. Seeger, *Int. J. Quantum Chem.*, 1976, **10**, 1–19.
29 C. Adamo, *J. Chem. Phys.*, 1999, **110**, 6158–6170.
30 X. Gao, S. Bai, D. Fazzi, T. Niehaus, M. Barbatti and W. Thiel, *J. Chem. Theory Comput.*, 2017, **13**, 515–524.
31 N. G. Connelly and W. E. Geiger, *Chem. Rev.*, 1996, **96**, 877–910.
32 J. Liu, K. Zhou, D. Wang, C. Deng, K. Duan, Q. Ai and Q. Zhang, *Front. Chem.*, 2019, **7**, 1–9.
33 M. Cai, M. Auffray, D. Zhang, Y. Zhang, R. Nagata, Z. Lin, X. Tang, C.-Y. Chan, Y.-T. Lee, T. Huang, X. Song, Y. Tsuchiya, C. Adachi and L. Duan, *J. Chem. Eng.*, 2021, **420**, 127591.
34 T. Serevičius, J. Dodonova, R. Skaisgiris, D. Banevičius, K. Kazlauskas, S. Juršėnas and S. Tumkevičius, *J. Mater. Chem. C*, 2020, **8**, 11192–11200.
35 M. K. Manna, S. Shokri, G. P. Wiederrecht, D. J. Gosztola and A. J. L. Ayitou, *Chem. Commun.*, 2018, **54**, 5809–5818.